Journal of Materials Science: Materials in Medicine (2025)36:4
https://doi.org/10.1007/s10856-024-06847-2

ENGINEERING AND NANO-ENGINEERING APPROACHES FOR MEDICAL DEVICES

Original Research

Zinc oxide nanoparticles decorated nitrogen doped porous reduced graphene oxide-based hybrid to sensitive detection of hydroxychloroquine in plasma and urine

Mohammad Amiri[1] · Zahra Hashemi[1] · Fereshteh Chekin[2]

Received: 25 May 2024 / Accepted: 26 November 2024

Abstract

The antimalarial hydroxychloroquine (HCQ) has considered for the treatment of systemic lupus erythematosus. Moreover, HCQ has been used as a drug to treat Coronavirus disease (COVID-19). In this work, nitrogen doped porous reduced graphene oxide (NprGO) has been prepared via environmentally friendly process using Fummaria Parviflora extract. A catalyst based on ZnO nanoparticles-nitrogen doped porous reduced graphene oxide (ZnO-NprGO) was prepared by hydrothermal method and characterized. The diameter of ZnO nanoparticles was ~22–37 nm, which were inserted between the NprGO sheets effectively prevented their aggregation. The ZnO-NprGO hybrid had high surface area and good electrocatalytic property, suiting for determination of HCQ. The ZnO-NprGO modified carbon paste electrode (CPE)-based sensor operated in a wide concentration range of 0.07–5.5 μmol L^{-1} with low limit of detection of 57 nmol L^{-1} and sensitivity of 14.175 μA μmol^{-1} L. Remarkably, the ZnO-NprGO/CPE sensor indicated acceptable accuracy, reproducibility, and stability. In addition, the proposed sensor was applied to detection of HCQ in biological samples and the recoveries were 92.0–102.5%, with relative standard deviations of 1.9–4.3%. The unique physical structure of ZnO-NprGO, as well as its chemical and electrical properties, make it promising interface for use in sensors and nanoelectronic applications.

Graphical Abstract

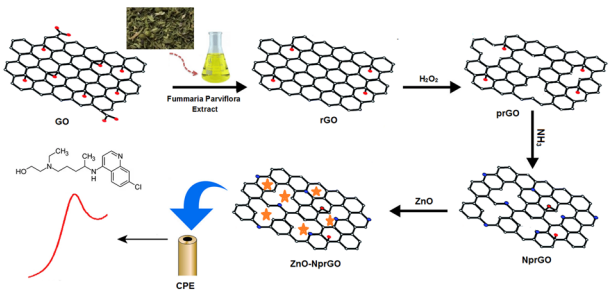

1 Introduction

COVID-19 is caused by coronavirus, which is associated to severe acute respiratory syndrome (SARS) and some common colds [1]. The COVID-19 caused over 5.8 million deaths worldwide until February 2022 [2], and to date, no certain drug has been found for the treatment of human coronavirus. Hydroxychloroquine (HCQ) has been used as a potential therapeutic drug for COVID-19 [3]. Also, hydroxychloroquine and ivermectin are included in COVID-19 kits as a pre-treatment option. However, no

✉ Fereshteh Chekin
fchekin@yahoo.com

[1] Department of Pharmacy, Ayatollah Amoli Branch, Islamic Azad University, Amol, Iran

[2] Department of Chemistry, Ayatollah Amoli Branch, Islamic Azad University, Amol, Iran

Published online: 07 January 2025

scientific evidence shows the effectiveness of HCQ to prevent COVID-19 infection [4, 5].

HCQ (antimalarial drug) is used initially to treat of *Plasmodium* parasitic infection. Beyond its antimalarial, HCQ has been operated in infectious and autoimmune diseases, and neoplastic and metabolic disorders [6]. HCQ as the most valuable therapeutic agent in systemic lupus erythematosus (SLE) shows multiple benefits associated with the disease itself and its related comorbidities. HCQ is available, inexpensive, and well-tolerated immunomodulatory [7]. All patients with SLE should be given HCQ unless there are side effects [8]. So, we should operate rapid, accurate, and selective analytical approach capable of using small sample volume with no interferences [9].

Recently, electrochemical electrodes due to fast, portable, and relatively cheap, and excellent ability to detect the electro-active species have been reported as powerful tools. Various conductive and non-conductive mediators such as reduced graphene oxide–TiO_2, ZnO nanoparticles, vanadium bisulfide quantum dots and etc. were suggested for HCQ analysis [10–12].

Graphene oxide (GO) and reduced graphene oxide (rGO) have a two-dimensional and planar structure with more available surface area for anchoring catalysts [13, 14]. In addition, GO and its derivatives have prominent biocompatibility, high carrier mobility, and wide potential window, so that the electron transfer rate is facilitated between the electrode and the active reaction. Thus, they are the desired substrates for anchoring catalysts in biosensors. The doping of nitrogen elements can improve the spin density, conductivity, active sites, and binding ability of graphene sheets [15, 16]. The pores in GO can effectively increase surface area and catalytically active sites for anchoring NPs, accordingly reducing the agglomeration of NPs. Moreover, the pore size and porosity fit with more species, increase the contact between a porous electrode and electrolyte, and shorten the transmission distance of different ions, thus improving the electro-catalytic activity [17, 18]. Zinc oxide (ZnO) is usually operated as a catalyst [19], gas sensor material [20], UV absorber [21], and pigment in cosmetics [22] and paints [23]. ZnO with various particle sizes and shapes can be synthesized by different processes [24–26]. ZnO nanoparticles with narrow particle size distribution and defined particle shape are used in advanced applications [27, 28]. Therefore, the synthesis and characterization of nanoscale ZnO have attracted tremendous attention of scientists.

The synthesis condition play a vital role in determining the features of nanoparticles to achieve the desired application. The various techniques such as ball milling, microemulsion, sol-gel, chemical co-precipitation, hydrothermal, and green methods were used for the synthesis of nanoparticles [29, 30]. The hydrothermal technique is a promising alternative synthetic method because of the low process temperature and very easy to control the particle size. The hydrothermal process has several advantages over other growth processes such as use of simple equipment, catalyst-free growth, low cost, large area uniform production, environmental friendliness, and less hazardous. This method has also been successfully employed to prepare nanoscale ZnO and other luminescent materials. The particle properties such as morphology and size can be controlled via the hydrothermal process by adjusting the reaction temperature, time and concentration of precursors [31].

In the present research, we designed an electrochemical tool based on ZnO-NprGO/CPE. The potential of ZnO-NprGO/CPE sensor for HCQ detection was investigated. This effort will open up new opportunities to develop novel electrochemical sensors for monitoring drugs.

2 Experimental

2.1 Reagents

The Fummaria Parviflora was prepared from local stores. Graphene oxide was obtained from Iranian Nano Materials Pioneers Co. (Mashhad, Iran). The all chemicals, such as hydroxychloroquine, zinc nitrate, potassium hexacyanoferrate (II), phosphoric acid and its salts, hydrogen peroxide, ammonia, carbon graphite powder were prepared from Sigma-Aldrich (Hamburg, Germany) and may be utilized without extra purification. Human plasma and urine were prepared from a clinical laboratory (Amol, Iran).

2.2 Apparatus

The morphology and topography were analyzed by MIRATESCAN-XMU scanning electron microscope (Czech Republic) combined with energy-dispersive X-ray spectrophotometer. Electrochemical measurments were carried out using Sama 500-c potentiostat/galvanostat (Iran). A cell consisting of a working electrode (modified CPE), a reference electrode ($Ag|AgCl|KCl_{(3M)}$), and an auxiliary electrode (platinum wire) was employed. UV-Vis analysis was carried out by UV-1900 UV-Vis spectrophotometer (Shimadzu Co., Japan). A Bruker D8-Advance X-ray diffractometer (Germany) was used for X-ray diffraction measurement. A Takram P50C0R10 Raman spectrometer (Teksan, Iran) was applied for Raman analysis.

2.3 Synthesis of ZnO-NprGO

rGO was synthesized according to our previous works [32, 33]. 10 g of fresh Fummaria Parviflora plant was mixed

with 100 mL of distilled water and placed in an ultrasound bath (60 kHz frequency) at 50 °C for 60 min. At least, the sample was filtered through a Whatman filter paper to obtain extract and stored at 4 °C. 10 mg GO was added to 50 mL extract and sonicated for 30 min in ultrasound bath. The mixture was refluxed at 50 ^{0}C for 6 h. The product (rGO) was washed using water, and dried in the oven at 100 °C. The porous rGO (prGO) was prepared based on a previous work [34]. 5 mg of synthesized rGO was sonicated in 5 mL of H_2O_2 (30%) for 30 min and refluxed for 10 h at 60 °C. The product (prGO) was washed with water. The nitrogen-doped porous reduced graphene oxide (NprGO) was prepared using ammonia [35, 36]. The prGO and ammonia (1:30 W/V) mixture was sonicated for 30 min. The mixture was heated for 10 h at 180 °C. The product was washed with ethanol and water, and dried in an oven at 60 °C overnight.

The zinc nitrate (5 mL, 0.1 M) and 10 mL of NprGO (1 mg/mL) were mixed and then 10 mL of Fummaria Parviflora extract was added drop by drop to the mixture at 70 °C for 1 h. The product (ZnO-NprGO) was washed with water, and heated at 350 °C for 2 h.

2.4 Fabrication of ZnO-NprGO/CPE

The CPE was fabricated according to previous reports [37]. Briefly, the graphite powder and paraffin were thoroughly hand-mixed and transferred into a glass tube with an internal radius of 3 mm. A copper wire was used to establish electrical contact. 1 mg of ZnO-NprGO was dispersed in ethanol (1 mL) by sonication for 30 min. Then, 5 µL of ZnO-NprGO was drop-casted onto CPE and dried in an oven at 50 °C.

2.5 Analysis of plasma and urine

500 µL of plasma or urine was added to 10 mL of buffer phosphate solution (PBS, pH = 7.0) and analyzed by

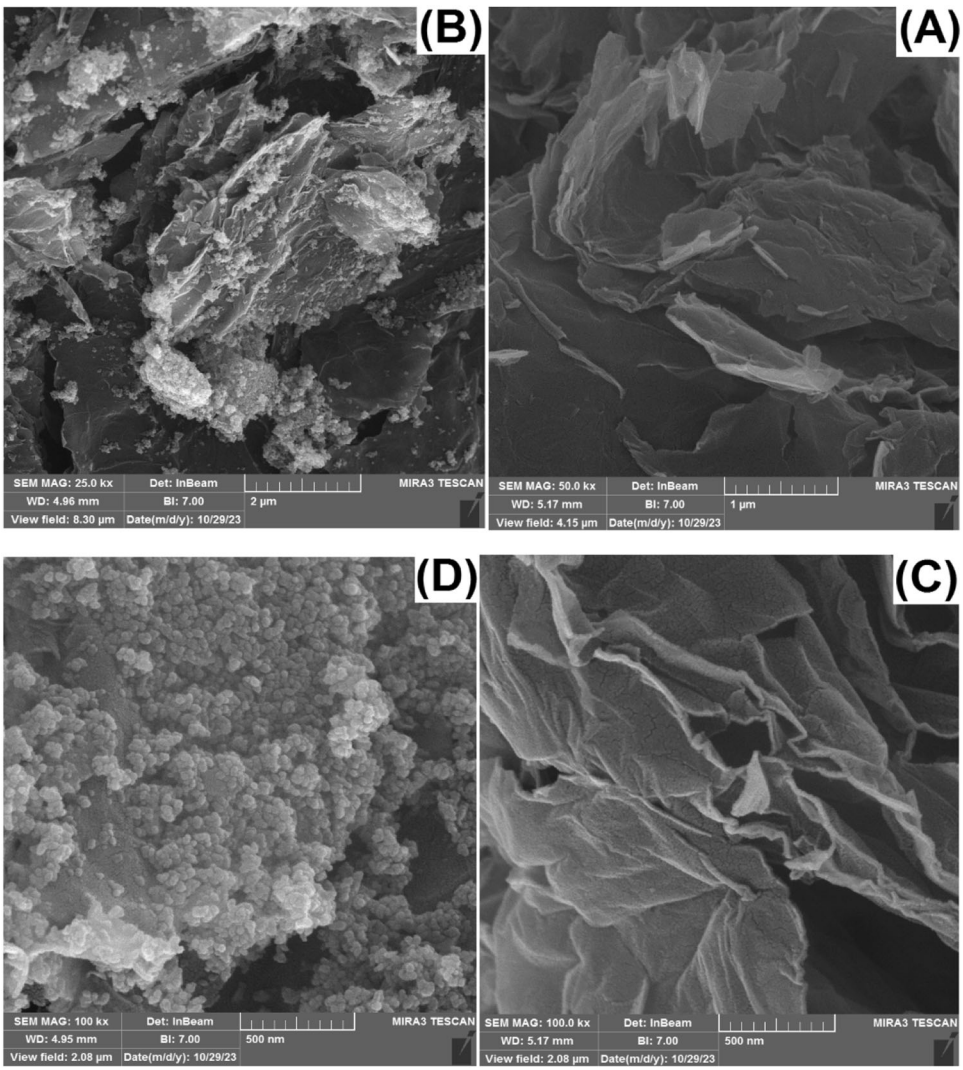

Fig. 1 FE-SEM images of NprGO (**A**, **C**) and ZnO-NprGO (**B**, **D**) with different magnitude

voltammetry method. Also, the samples were analyzed at the wavelength of 330 nm by UV-Vis spectroscopy with the addition of 500 µL in 4 mL PBS.

3 Results

3.1 Characterization

Figure 1 shows the FE-SEM images of NprGO and ZnO-NprGO samples. As seen, the NprGO is wave-shaped corrugated structure and multilayered sheets. In contrast, ZnO-NprGO depicts the formation of sphere-shaped nanoparticles of ZnO with a nanometer scale (22–37 nm). The EDS spectrum indicates the existence of C, O, and N elements in NprGO (Fig. 2A) and C, O, N and Zn elements in ZnO-NprGO (Fig. 2B) confirming the formation of ZnO-NprGO nanostructure.

Powder X-ray diffraction (XRD) is an effective analytical technique to study the changes of interlayer and crystal structures of samples. Figure 3A shows the XRD pattern of NprGO and ZnO-NprGO. As observed, NprGO indicates the peaks at 26.6°, and 47.7 related to the (002) and (100) reflections, while the diffraction peaks at 32.2, 34.6, 36.4, 47.9, 56.7, 63.3, 66.9, 68.1, 69.5, 73.2 and 77.3° could be indexed to the (100), (002), (101), (102), (110), (103), (200), (112), (201), (004) and (202) planes of the wurtzite hexagonal zinc oxide (JCPDS36-1451) [38].

Raman spectra of NprGO and ZnO-NprGO are shown in Fig. 3B. The NprGO exhibited the D and G bands at 1367 cm^{-1} and 1598 cm^{-1}, attributed to defects in the graphitic layers and sp^2 carbon structure, respectively [39]. The ZnO-prGO exhibited a decreased intensity ratio (0.95) between peaks (I_D/I_G) compared with NprGO (0.99). In addition, the D and G bands in ZnO-NprGO shifted to higher frequencies (1388 cm^{-1} and 1619 cm^{-1}). The peaks at 329, 428 and 1066 cm^{-1} are assigned to E2(High)–E1(low), E2(high) and 2A1(low) modes of ZnO, respectively [40].

The evidence of formed NprGO and ZnO-NprGO is investigated by UV-Vis spectra in wavelength range of 200–600 nm (Fig. 4A). An absorption broad peak was observed at ~260 nm for NprGO. The absorption peaks of 260 and 369 nm in ZnO-NprGO spectrum belong to NprGO and ZnO nanoparticles respectively, confirming the synthesis of ZnO-NprGO hybrid.

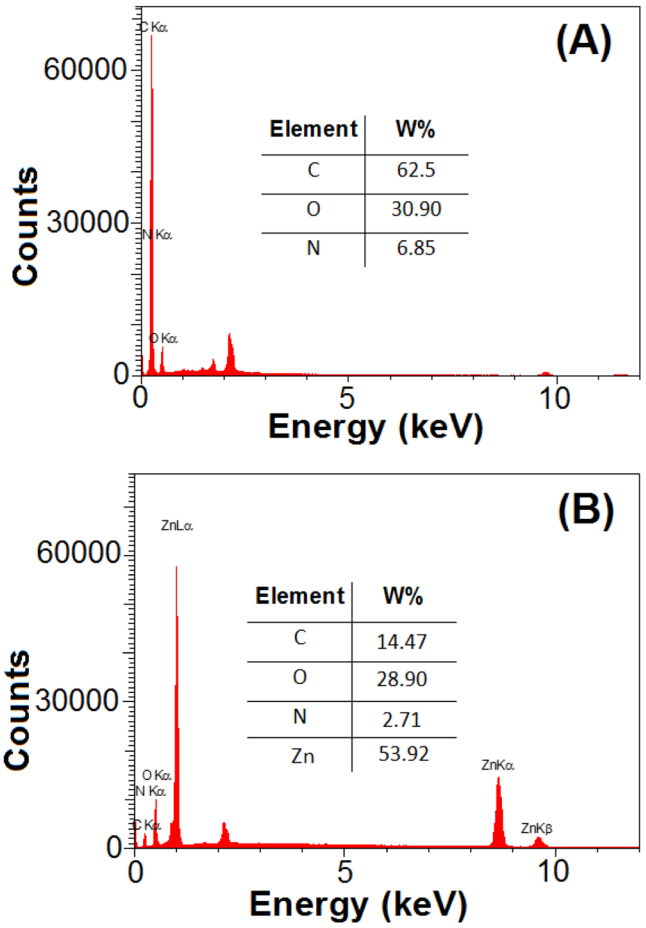

Fig. 2 EDS spectra of **A** NprGO and **B** ZnO-NprGO

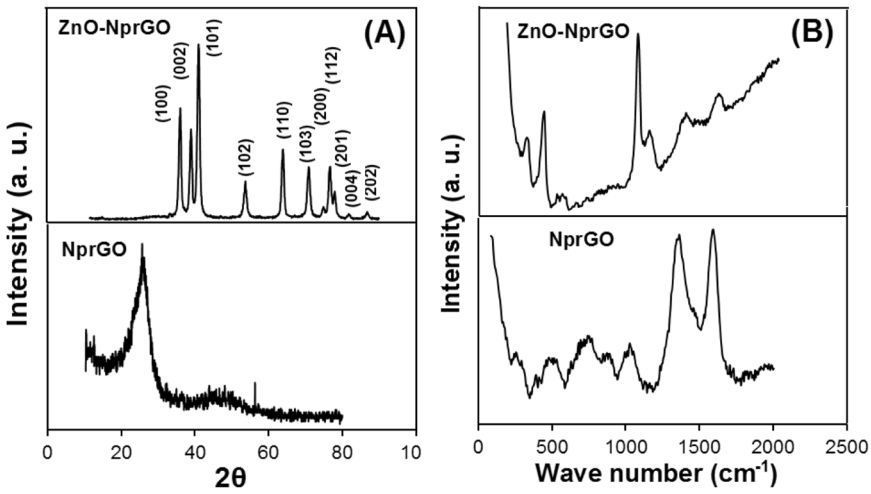

Fig. 3 **A** XRD patterns and **B** Raman spectra of NprGO and ZnO-NprGO

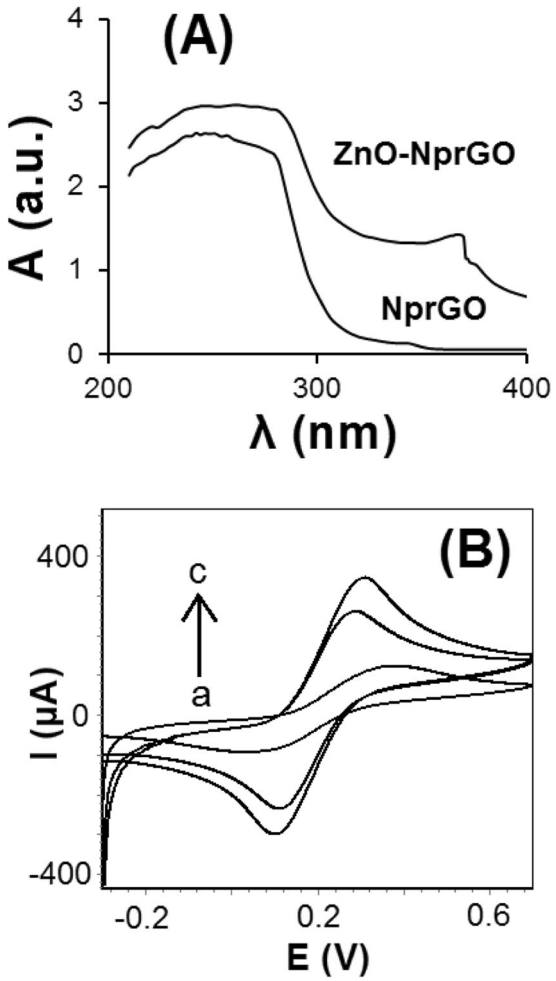

Fig. 4 **A** UV-Vis spectra of NprGO and ZnO-NprGO solution (1 mg/mL). **B** Cyclic voltammograms of (a) CPE, (b) NprGO/CPE and (c) ZnO-NprGO/CPE using $[Fe(CN)_6]^{3-/4-}$ (3 mmol L^{-1})/PBS (0.1 mol L^{-1})

The electrical response of bare CPE, NprGO/CPE, and ZnO-NprGO/CPE was studied in $[Fe(CN)6]^{3-/4-}$ using cyclic voltammetry (Fig. 4B). The redox peak current increased significantly on ZnO-NprGO/CPE in comparison with those recorded for NprGO/CPE and CPE. The architecture of the ZnO-NprGO hybrid generates a larger electroactive surface area, resulting in higher current. The good electronic properties of NprGO, and ZnO facilitating fast electron transfer, by a porous structure cause the current enhancement. The electroactive surface area of CPE, NprGO/CPE, and ZnO-NprGO/CPE was calculated from the slope of plotting the peak current of $[Fe(CN)_6]^{4-}$ (3 mmol L^{-1}) vs. the square root of the scan rate using Eq. 1 [41]:

$$A = \text{slope}/(268.6 \times n^{3/2} \times D^{1/2} \times C) \quad (1)$$

where A, n, D, and C are the electroactive surface area (cm^2), number of transferred electrons ($n = 1$), diffusion coefficient, and concentration of $[Fe(CN)_6]^{4-}$, respectively. In contrast to CPE (0.07 cm^2) and NprGO/CPE (0.14 cm^2), ZnO-NprGO/CPE shows a higher effective surface area (0.17 cm^2), indicating ZnO-NprGO hybrid as electrode material.

3.2 Voltammetric study of hydroxychloroquine

The cyclic voltammograms of CPE, NprGO/CPE and ZnO-NprGO/CPE are shown in 0.1 mol L^{-1} PBS with pH=7.0 containing 15 μmol L^{-1} HCQ (Fig. 5A). As seen, a small board oxidation peak of HCQ on surface of CPE is observed, while oxidation potentials of HCQ at NprGO/CPE and ZnO-NprGO are shown at 0.836 V and 1.051 V. The NprGO nanosheets in electronic and synergistic association with ZnO nanoparticles might be due to the high surface. In addition, the results showed that the ZnO-NprGO/CPE presents higher conductivity and oxidation current for HCQ.

The pH of the PBS affects the oxidation current of HCQ. The voltammetric oxidation of HCQ was examined that

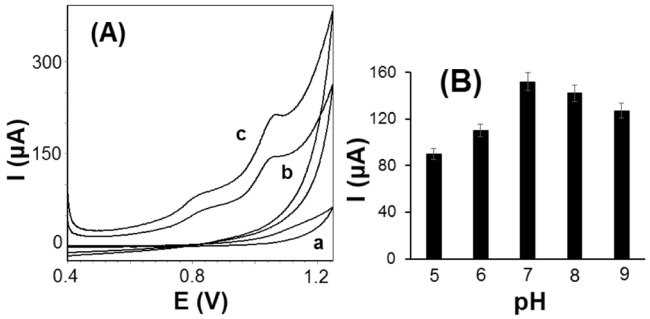

Fig. 5 **A** Cyclic voltammograms of 25 μmol L^{-1} HCQ at scan rate of 100 mV s^{-1} at surface of (a) CPE, (b) NprGo/CPE and (c) ZnO-NprGO/CPE in 0.1 mol L^{-1} PBS (pH 7.0). **B** Plot of peak current of 15 μmol L^{-1} HCQ in 0.1 mol L^{-1} PBS at the surface of ZnO-NprGO/CPE at various pH at scan rate of 100 mV s^{-1}

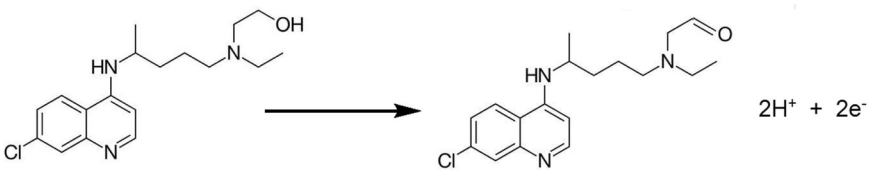

Scheme 1 The electrooxidation mechanism of HCQ.

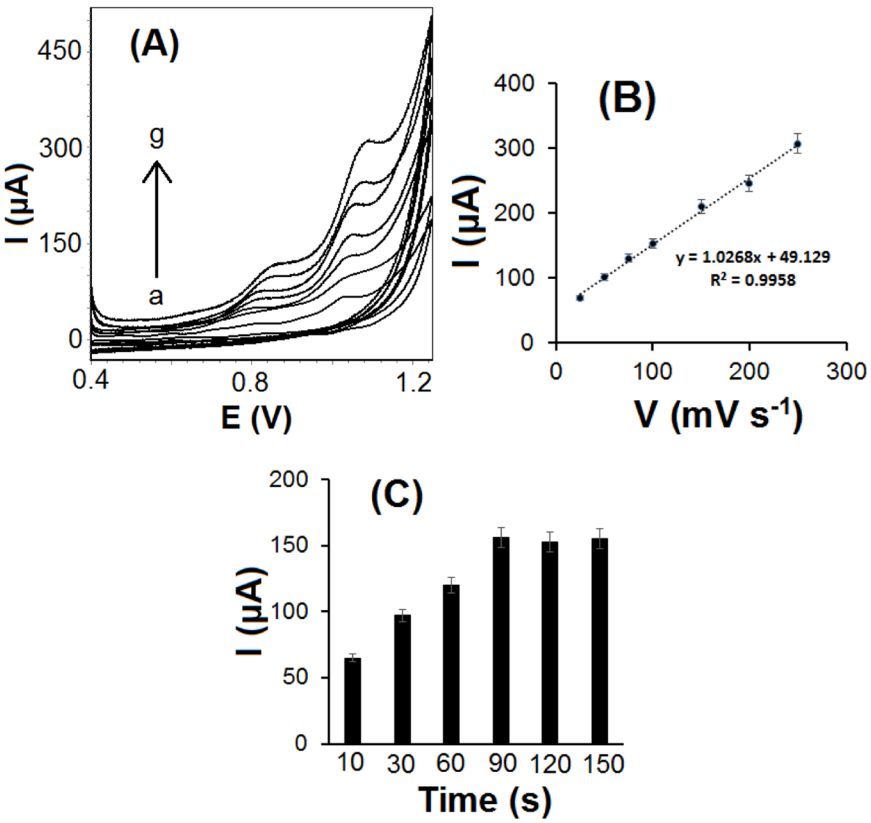

Fig. 6 **A** cyclic voltammograms of 15 μmol L^{-1} HCQ in 0.1 mol L^{-1} PBS (pH 7.0) and 0.1 mol L^{-1} KCl as supporting electrolyte at the surface of ZnO-NprGO/CPE at various scan rates: **a** 25, **b** 50, **c** 75, **d** 100, **e** 150, **f** 200 and **g** 250 mV s^{-1}; **B** Plot of peak currents vs. scan rates; **C** Plot of peak current 15 μmol L^{-1} HCQ in 0.1 mol L^{-1} PBS at the surface of ZnO-NprGO/CPE at various adsorption time at scan rate of 100 mV s^{-1}

peak current increased from 4.0 to 7.0, where it reached a maximum value (Fig. 5B). Therefore, pH 7.0 was selected as the suitable pH for further tests. It's found that the same number of electrons and protons (Scheme 1) participates in electro-oxidation of HCQ.

The scan rate effect on electro-oxidation of HCQ in PBS (0.1 mol L^{-1}, pH 7.0) was studied in range 25–250 mV s^{-1} (Fig. 6A). The HCQ oxidation current increased with increasing scan rates, while the oxidation potential shifted towards positive direction with the increase of the scan rate. The plot of the oxidation current vs. square root of scan rate was found a linear relationship (Fig. 6B), indicating an adsorption-controlled reaction. Further, the adsorption behavior of HCQ on ZnO-NprGO/CPE makes the adsorption time (t) crucial parameter for detection. The oxidation current was also improved with increase in time up to 90 s (Fig. 6C). So, the electrode surface is saturated at 90 s time.

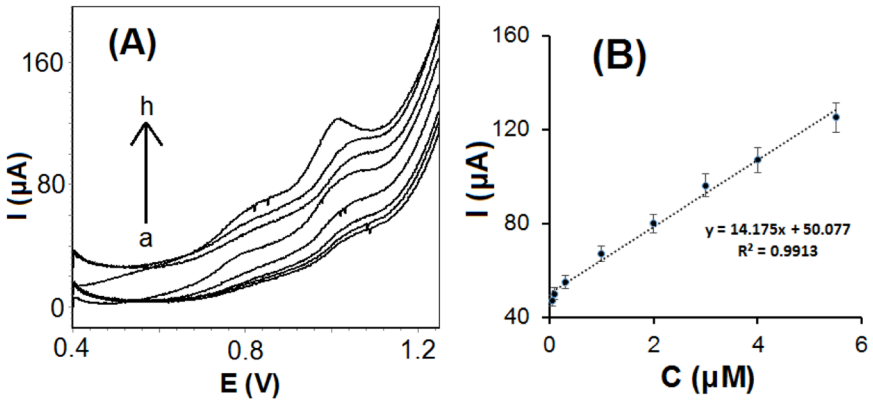

Fig. 7 **A** Squar wave voltammograms obtained ZnO-NprGO/CPE in the presence of (**a**) 0.07, (**b**) 0.1, (**c**) 0.3, (**d**) 1, (**e**) 2, (**f**) 3, (**g**) 4 and (**h**) 5.5 μmol L^{-1} HCQ; **B** Calibration curve of peak currents vs. concentration of HCQ

Table 1 Analytical parameters for voltammetric determination of HCQ at different modified electrodes

Electrode	Method	Linear range (μmol L^{-1})	LOD (nmol L^{-1})	Sensitivity (μA μmol L^{-1})	Ref.
ZnO/CPE	DPV[a]	0.8–1000	133	4.52	11
VS2QDs[b]/GCE	DPV	0.84–22.50	2.80	8.93	12
BDD[c]	SWV	0.10–1.9	60	1.24	42
MWCNT/CPE	ASDPV[d]	0.57–100	6	0.37	43
SPE[e]	DPV	0.42–7.50	40	0.31	44
GCE[f]	DPV	0.01–11.90	5	0.21	45
PMDASAM[g]/GCE	DPV	0.09–10.20	5	–	46
ZnO-NprGO/CPE	SWV	0.07–5.50	57	14.17	this work

[a]Differential pulse voltammetry

[b]Vanadium disulfiede quantum dots

[c]Boron doped diamond

[d]Adsorptive stripping differential pulse voltammetry

[e]Screen printed electrode

[f]Glassy carbon electrode

[g]N,N-bis[(E)-(1-pyridyl)methylidene]-1,3-propanediamine self-assembled monolayer

3.3 Validation of ZnO-NprGO/CPE sensor

The measurment of HCQ was launched based on the peak current vs. HCQ concentration. Square wave voltammograms (SWV) present the increase in peak current vs. HCQ concentration in the range 0.07–5.5 μmol L^{-1} at ZnO-NprGO/CPE (Fig. 7A). Limit of detection (LOD) of HCQ was estimated from LOD = 3σ /b, where σ is the standard deviation of the blank and b is the slope of the calibration curve and was found 57 nmol L^{-1}. The sensitivity was calculated 14.175 μA μmol^{-1} L. The LOD, LDR and sensitivity (Table 1) confirmed the precision of ZnO-NprGO/CPE in comparison with other sensors presented in Table 1 [11, 12, 42–46].

The repeatability and intermediate precision were investigated by measuring five successive tests for 15 μmol L^{-1} HCQ. The RSD values were estimated to be 2.7 and 3.3% for one day (intra-assay) and seven days (inter-assay) respectively, which indicate excellent repeatability.

Interference studied is a good approach for determining the selectivity of ZnO-NprGO/CPE to detection HCQ. The interference tests were carried out by adding some common interfering species such as cysteine, acetaminophen, lysine, glucose, Na^+, K^+, Cl^-, ascorbic acid, uric acid and sucrose as common interferences in biological samples. The assay of 15 μmol L^{-1} HCQ was examined by the addition of 75 μmol L^{-1} interferences. The results obtained showed no significant change in the HCQ current in the presence of the mentioned interferents, indicating high selectivity of the proposed sensor toward HCQ (Fig. 8A).

3.4 Assay of biological samples

To evaluate the applicability and validity of the proposed sensor, recovery experiments were monitored with HCQ analysis in known amounts to human plasma and urine. The mean recoveries and RSD values of HCQ were found to be 92.0–102.0% and 1.9–4.3%, respectively (Table 2). Moreover, HCQ analysis in human plasma and urine was

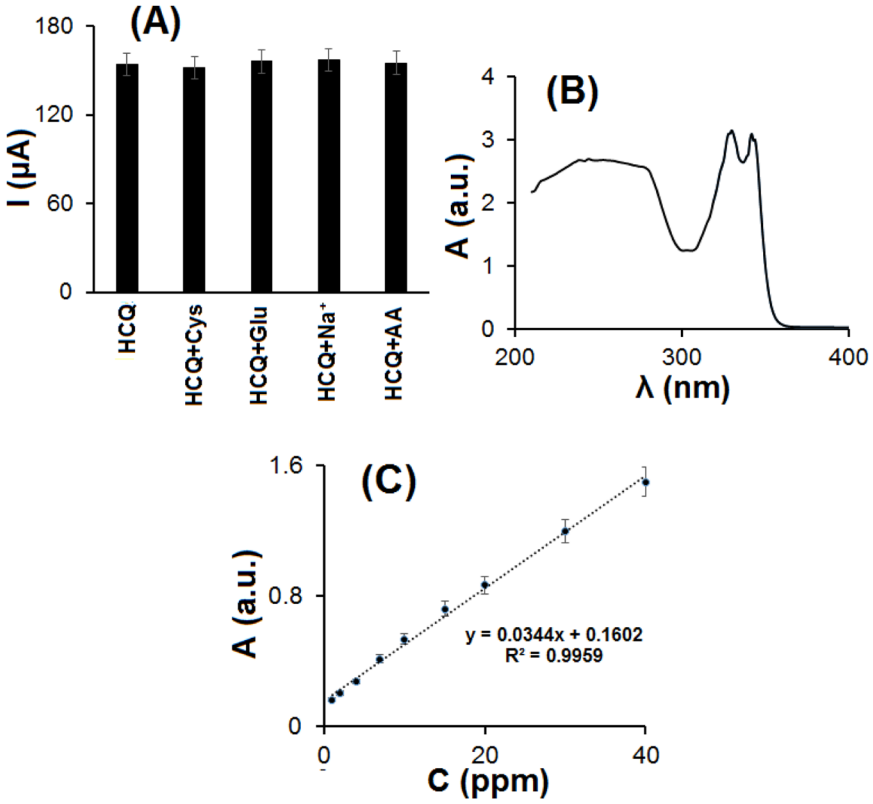

Fig. 8 **A** Detected current of 15 µmol L^{-1} HCQ by CV at ZnO-NprGO/CPE in PBS (pH 7.0) upon the addition of 75 µmol L^{-1} cysteine (Cys), glucose (Glu), Na^{+} and ascorbic acid (AA); **B** The UV-Vis spectrum of 100 ppm HCQ in PBS (pH 7.0); **C** calibration curve of HCQ determined by UV-Vis spectroscopy

Table 2 Determination of HCQ in urine and plasma samples at surface of ZnO-NprGO/CPE in 0.1 mol L^{-1} PBS solution (pH 7.0)

Sample	Added (µmol L^{-1})	Found (µmol L^{-1})	Mean recovery (%) ($n = 3$)	
			Proposed method	UV method
Plasma	5.0	4.6	92.0 ± 1.9	99.7 ± 4.5
Plasma	10.0	9.3	93.0 ± 2.1	97.7 ± 3.6
Urine	5.0	5.1	102.0 ± 2.9	96.9 ± 1.5
Urine	10.0	9.6	96.0 ± 4.3	98.1 ± 3.3

performed by UV-Vis spectroscopy (Fig. 8B, C). The data reported in Table 2 showed that the electrochemical results don't significantly differ from UV-Vis spectroscopy. So, the ZnO-NprGO/CPE is well adapted for sensing of HCQ.

4 Discussion

The current innovation relates to green production ZnO nanoparticles and ZnO-NprGO nanocomposite employing Fummaria Parviflora extract as a reducing agent. Because of graphene oxide and its derivatives remarkable physiochemical properties, such as their huge surface area, good biocompatibility, and low toxicity, graphene nanocomposites have gotten a lot of interest [13]. The graphene nanocomposites due to their biomedical properties can be used in various applications, such as sensors and pharmaceuticals [14]. As a result, a method of generating metal oxide and graphene nanocomposites using Fummaria Parviflora extract is desired.

The rGO was result of GO conversion using reduction method or the addition of reducing agents that aim to eliminate the oxygen functional groups found along the GO plane [32]. Research carried out has succeeded in reduce GO using Fummaria Parviflora as a reduction agent. In green synthesis, various natural materials such leaf extracts, peels, bio-compounds and microbes is used as reducing agent [33]. Fummaria Parviflora contains high levels of phenolic acids and flavonoids, which allow to act as reducing agent as well as stabilizing agent [47].

Recent studies have shown that porous graphene should also, be very useful as new support because of porous supports can not only provide high surface area but also facilitate the diffusion and mass transport of reactants [41]. Substitutional doping of graphene with heteroatoms could modify the chemical reactivity, electrical conductivity, and surface activity of graphene material. The results showed that the doping using nitrogen and sulfur atoms in GO material was successfully carried out [16]. One of the most researched inorganic metal oxide, ZnO is known to be biofriendly, non-toxic, thermally stable, and electrochemically active. Various nanostructures with the combination of

ZnO, have been widely used in the development of N_2H_4 sensor, and glucose and H_2O_2 biosensors [24].

For decades, the prevention and treatment of malaria have been significantly assisted by the use of the very efficient anti-malarial medication HCQ [6]. Since there is presently no specific therapeutic vaccination or antiviral medication accessible, HCQ can be utilized to treat the new Corona virus 2019 (Covid-19) infection in these situations [5]. Assertive negative effects or build-up of intoxication may also result from long-term HCQ usage [6]. Due to this, it's important to medically monitor HCQ plasma levels to optimize treatment and control negative effects. It is urgent and necessary to develop a quick, accurate, and user-friendly analytical technique to detect and quantify HCQ in pharmaceutical and biological samples. Electro-chemical sensors might be an excellent option to the detection of HCQ.

Our research has focused on using ZnO and NprGO which, represents an important and interesting semi-conductor due to its electrocatalytic activity for the analysis of HCQ in electrochemical sensors. This hybrid composite offer several advantages, including a large surface area, superior electrical conductivity, and simple preparation. The evidence of synthesized ZnO-NprGO composite was investigated by FE-SEM images, EDS, XRD, Raman and UV-Vis spectra, and cyclic voltammetry (Figs. 1–4). The ZnO-NprGO depicts the formation of sphere-shape nano-particles of ZnO with a diameter of 22–37 nm on NprGO sheets in good agreement with JCPDS89-0510 card. Si et al have fabricated ZnO/graphene on glassy carbon electrode to determine ofloxacin [48]. Wang et al have developed ZnO nanorods and graphene nanosheets on ITO glass for electrochemical sensing of uric acid in the presence of ascorbic acid [49]. For the electrochemical detection of organophosphorous pesticides, Liu et al have developed ZnO-rGO nanocomposite based-electrochemical biosensor [50]. Jin Choi et al have also developed ZnO-rGO nanocomposites toward NO_2 gas detection [51].

ZnO-NprGO demonstrated effective electro-catalytic activity to detect HCQ, and the oxidation current was significantly increased compared to alone ZnO and NprGO (Fig. 5). It is found that the pH 7.0 is as the suitable pH in determination of HCQ and the same number of electrons and protons participated in electro-oxidation of HCQ (Scheme 1). Also, the scan rate effect on electro-oxidation of HCQ indicated an adsorption-controlled reaction (Fig. 6A). The LDR, LOD, and sensitivity of HCQ on proposed sensor were calculated at 0.07–5.5 μmol L^{-1}, 57 nmol L^{-1} and 14.175 μA μmol^{-1} L, respectively.

Zhang et al. developed a simply sensitive sensor based on rGO–TiO2 nanocomposite-modified GCE was developed for the electrochemical determination of an anti-malarial drug, HCQ. A linear relationship between the peak current and the concentration was obtained, ranging from 0.25 to 500 μmol L^{-1} with the LOD of 12.5 nmol L^{-1} and sensitivity of 0.39 μA μmol^{-1} L [10]. Zoubir et al established a simple platform for electrocatalytic detection of hydroxychloroquine in human urine samples and pharmaceutical samples (tablets) using a ZnO@CPE sensor constructed by simple and inexpensive hydrothermal methods using a square wave voltammetry method. Under the optimized experimental conditions, the ZnO@CPE sensor showed good analytical performance for the determination of trace amounts of HCQ, a wide linearity range 0.8–1000 μmol L^{-1} with LOD of 133 nmol L^{-1} and sensitivity of 4.52 μA μmol^{-1} L. The calculated recovery and coefficient of variation for the two samples analyzed are very satisfactory, ranging from 97.6 to 102% and 1.2 to 2.3% respectively [11]. El-Wekil suggested an innovative electrochemical sensor based on vanadium disulfide quantum dots and insertion within N, S graphene aerogel and carbon nanotube nanaostructure for simultaneous voltammetric analysis of azithromycin and HCQ. This sensor showed a dynamic linear range of 0.08–0.30 μmol L^{-1} for analysis of HCQ with LOD of 3.0 nmol L^{-1} and sensitivity of 8.93 μA μmol^{-1} L [12].

As presented in Table 1, ZnO-NprGO/CPE shows many advantages such as simplicity, rapidity, cost effective, low LOD, and higher sensitivity in comparison with other works. LODs are however lower as compared to MWCNT/CPE [43], SPE [44], and PMDASAM/GCE [46]. The ease and one-step procedure of making ZnO-NprGO/CPE, as shown in this work, might be however an advantage when it comes for sensing in clinical samples. Moreover, there is no proof that a single electrode can work for a long period of time with almost the same performance, which gives the ZnO-NprGO/CPE the privilege of being used for routine work. In addition, the ZnO-NprGO might be functionalized to selectively determine different kinds of analytes.

The mean recoveries and RSD values of HCQ were found to be 92.0–102.0% and 1.9–4.3%, respectively, in human plasma and urine. Based on these results, the proposed electrode suggested for analysis of HCQ is reliable for quantification of HCQ with robust results. Moreover, the samples were analyzed by UV-Vis method, and it was found that no significant difference between the proposed and UV-Vis methods. Consequently, the proposed sensor is accurate for HCQ assay in human serum and urine samples with high accuracy.

5 Conclusion

The stable ZnO-NprGO hybrid was effectively synthesized via environmentally friendly process using extract. The high surface area and excellent conductivity were created

by combining NprGO sheets and ZnO particles. A rapid and accurate SWV method was operated to measure HCQ in biological samples. This method presents ZnO-NprGO-based CPE sensor. The ZnO-NprGO/CPE exhibited fast and stable response with extremely low LOD, wide LDR, and high sensitivity values due to ZnO successful adherence to NprGO that causes good electrical conductivity. Moreover, the ZnO-NprGO/CPE can be useful to detect HCQ in urine and human serum, suggesting the proposed method might be effective and reliable for HCQ sensing in real samples.

Acknowledgements The authors thank the facilities provided to carry out research at Ayatollah Amoli Branch of the Islamic Azad University.

Compliance with ethical standards

Conflict of interest The author declares no competing interests.

Publisher's note Springer Nature remains neutral with regard to jurisdictional claims in published maps and institutional affiliations.

References

1. Cucinotta D, Vanelli M. WHO declares COVID-19 a pandemic. Acta Biomed Atenei Parmensis. 2020;91:157–60.
2. Feng W, Newbigging AM, Le C, Pang B, Peng H, Cao Y, et al. Molecular diagnosis of COVID-19: challenges and research needs. Anal Chem. 2020;92:10196–209.
3. Gao J, Tian Z, Yang X. Breakthrough: Chloroquine phosphate has shown apparent effcacy in treatment of COVID-19 associated pneumonia in clinical studies. Biosci Trends. 2020;14:72–3.
4. Satarker S, Ahuja T, Banerjee M, E VB, Dogra S, Agarwal T, et al. Hydroxychloroquine in COVID-19: potential mechanism of action against SARS-CoV-2. Curr Pharm Rep. 2020;6:203–11.
5. Yao X, Ye F, Zhang M, Cui C, Huang B, Niu P, et al. In vitro antiviral activity and projection of optimized dosing design of hydroxychloroquine for the treatment of severe acute respiratory syndrome coronavirus 2 (SARS-CoV-2). Clin Infect Dis. 2020;71:732–9.
6. Olsen NJ, Schleich MA, Karp DR. Multifaceted effects of hydroxychloroquine in human disease. Semin Arthritis Rheum. 2013;43:264–72.
7. Dima A, Jurcut C, Arnaud L. Hydroxychloroquine in systemic and auto-immune diseases: where are we now. Jt Bone Spine. 2021;88:105143.
8. Dima A, Jurcut C, Chasset F, Felten R, Arnaud L. Hydroxychloroquine in systemic lupus erythematosus: overview of current knowledge. Ther Adv Musculoskelet Dis. 2022;14:1–25.
9. El-Wekil MM, Mahmoud AM, Marzouk AA, Alkahtani SA, Ali R. A novel molecularly imprinted sensing platform based on MWCNTs/AuNPs decorated 3D starfsh like hollow nickel skeleton as a highly conductive nanocomposite for selective and ultrasensitive analysis of a novel pan-genotypic inhibitor velpatasvir in body fluids, J Mol Liq. 2018;271:105–11.
10. Zhang H, Cheng L, Shang H, Zhang W, Zhang A. A Novel electrochemical sensor based on reduced graphene oxide–TiO_2 nanocomposites with high selectivity for the determination of hydroxychloroquine. Russ J Electrochem 2021;57:872–84.
11. Zoubir J, Bakas I, Qourza S, Tamimi M, Assabbane A. Electrochemical sensor based on a ZnO-doped graphitized carbon for the electrocatalytic detection of the antibiotic hydroxychloroquine, Application: tap water and human urine. J Appl Electrochem. 2023;53:1279–94.
12. Mater Mahnashi H, Mahmoud AM, Saad Alkahtani A, El-Wekil MM. Simultaneous electrochemical detection of azithromycin and hydroxychloroquine based on VS2QDs embedded N, S@graphene aerogel/cCNTs3D nanostructure. Microchem J. 2021;163:105925.
13. Wei Q, Wu L, Zhu M, Wang Zh, Huang ZhH, Wang MX. Porous nitrogen-doped reduced graphene oxide-supported CuO@Cu_2O hybrid electrodes for highly sensitive enzyme-free glucose biosensor. iScience 2023;26:106155.
14. Das P, Ibrahim SK, Chakraborty K, Ghosh S, Pal T. Stepwise reduction of graphene oxide and studies on defect-controlled physical properties. Sci Rep. 2024;14:294.
15. Rahsepar M, Foroughi F, Kim H. A new enzyme-free biosensor based on nitrogen-doped graphene with high sensing performance for electrochemical detection of glucose at biological pH value. Sens Actuator B Chem. 2019;282:322–30.
16. Mutadak PR, Warule SS, Kolhe PS, Bankar PK, More MA. Nitrogen doped reduced graphene oxide: Investigations on electronic properties using X-ray and Ultra-violet photoelectron spectroscopy and field electron emission behaviour. Surf Inter. 2023;41:103251.
17. Zhao Y, Bo X, Guo L. Highly exposed copper oxide supported on three-dimensional porous reduced graphene oxide for non-enzymatic detection of glucose. Electrochim Acta. 2015;176:1272–9.
18. Zhang Y, Wan Q, Yang N. Recent advances of porous graphene: synthesis, functionalization, and electrochemical applications. Small. 2019;15:e1903780–818.
19. Jabar MF. Synthesis and characterisation of zinc oxide catalyst and its composite with polymer additives. Mater Sci Eng. 2020;870:012023.
20. Junfeng Chao J, Yu H, Zhang K, Zhou Y, Meng D, Sun Y. Integration of ZnO and Au/ZnO nanostructures into gas sensor devices for sensitive ethanolamine detection. ACS Appl Nano Mater. 2023;6:5994–6001.
21. Youssef AM, El-Nagar IE, El Torky AMM, Abd El Haakim AA. Development and characterization of CMC/PVA films loaded with Zno-nanoparticles for antimicrobial packaging application. Der Pharma Chem. 2017;9:157–63.
22. Ma J, Zhu W, Tian Y, Wang Z. Preparation of Zinc Oxide-starch nanocomposite and its application on coating nanoscale. Res Lett. 2016;11:200–9.
23. Foudi H, Soukeur A, Rekhila G, Trari M, Amara M. Synthesis and characterization of ZnO nanoparticles for antibacterial paints. Chem Pap. 2023;77:1489–96.
24. Dhoke SHK. Synthesis of nano-ZnO by chemical method and its characterization. Results Chem. 2023;5:100771.

25. Gamedze NP, Mthiyane DMN, Mavengahama S, Singh N, Onwudiwe DC. Biosynthesis of ZnO nanoparticles using the aqueous extract of mucuna pruriens (utilis): Structural characterization, and the anticancer and antioxidant activities. Chem Afr. 2024;7:219–28.
26. Ahmed Abdullah JA, Jiménez Rosado M, Guerrero A, Romero A. Eco-friendly synthesis of ZnO-nanoparticles using *Phoenix dactylifera* L., polyphenols: physicochemical, microstructural, and functional assessment. N. J Chem. 2023;47:4409–17.
27. Khan M, Ahmad B, Hayat KH, Ullah F, Sfina N, Elhadi M, Khan AA, Husain M, Rahman N. Synthesis of ZnO and PEG-ZnO nanoparticles (NPs) with controlled size for biological evaluation. RSC Adv. 2024;14:2402–9.
28. Jabir MS, Al-Shammari AM, Ali ZO, Albukhaty S, Sulaiman GM, Jawad SF, Hamzah SS, Syed A, Elgorban AM, Eswaramoorthy R, Zaghloul NSS, Al-Dulimi A, Najm MAA. Combined oncolytic virotherapy gold nanoparticles as synergistic immunotherapy agent in breast cancer control. Sci Rep. 2023;13:16843.
29. Nadhiya D, Kala A, Sasikumar P, Mohammed MKA, Thirunavukkarasu P, Prabhaharan M, Karnan C, Albukhaty S, Jabir MS, Syed A, Elgorban AM, Zaghloul NSS. Influence of Cu^{2+} substitution on the structural, optical, magnetic, and antibacterial behaviour of zinc ferrite nanoparticles. J Saudi Chem Soc. 2023;27:101696.
30. Aziz Neamah S, Albukhaty S, Qusay Falih I, Hassan Dewir Y, Mahood HB. Biosynthesis of zinc oxide nanoparticles using capparis spinosa L. fruit extract: Characterization, biocompatibility, and antioxidant activity. Appl Sci. 2023;13:6604.
31. Bulcha B, Tesfaye JL, Anatol D, Shanmugam R, Dwarampudi LP, Nagaprasad N, Nirmal Bhargavi VL, Krishnaraj R. Synthesis of zinc oxide nanoparticles by hydrothermal methodsand spectroscopic investigation of ultraviolet radiation protective properties. J Nanomater. 2021;2021:617290.
32. Vatandost E, Ghorbani-HasanSaraei A, Chekin F, Naghizadeh Raeisi SH, Shahidi SA. Green tea extract assisted green synthesis of reduced graphene oxide: Application for highly sensitive electrochemical detection of sunset yellow in food products. Food Chem X. 2020;6:100085–90.
33. Vatandost E, Ghorbani-HasanSaraei A, Chekin F, Naghizadeh Raeisi SH, Shahidi SA. Antioxidant, antibacterial and anticancer performance of reduced graphene oxide prepared via green tea extract. Chem Sel. 2020;5:10401–6.
34. Chekin F, Singh SK, Vasilescu A, Dhavale VM, Kurungot S, Boukherroub R, Szunerits S. Reduced graphene oxide modified electrodes for sensitive sensing of Gliadin in food samples. ACS Sens. 2016;1:1462–70.
35. Chekin F, Myshin V, Ye R, Melinte S, Singh SK, Kurungot S, Boukherroub R, Szunerits S. Graphene-modified electrodes for sensing doxorubicin hydrochloride in human plasma. Anal Bioanal Chem. 2019;411:1509–16.
36. Chekin F, Vasilescu A, Jijie R, Singh SK, Kurungot S, Iancu M, Badea G, Boukherroub R, Szunerits S. Sensitive electrochemical detection of cardiac troponin I in serum and saliva by nitrogen-doped porous reduced graphene oxide electrode. Sens Actuators B. 2018;262:180–7.
37. Zareyy B, Chekin F, Fathi SH. NiO/porous reduced graphene oxide as active hybrid electrocatalyst for oxygen evolution reaction. Russ J Electrochem. 2019;55:333.
38. Manjunatha CH, Chirag V, Wali Shivaraj B, Srinivasa N, Ashoka S. One pot green synthesis of novel rGO@ZnO nanocomposite and fabrication of electrochemical sensor for ascorbic acid using screen-printed electrode. J Nanostruct. 2020;10:531–9.
39. Schuepfer DB, Badaczewski F, Guerra-Castro JM, Hofmann DM, Heiliger CH, Smarsly B, Klar PJ. Assessing the structural properties of graphitic and non-graphitic carbons by Raman spectroscopy. Carbon. 2020;161:359–72.
40. Rodwihok CH, Wongratanaphisan D, Thi Ngo YL, Khandelwal M, Hyun Hur S, Chung JS. Effect of GO additivein ZnO/rGO nanocomposites with enhanced photosensitivity and photocatalytic activity. Nanomater. 2019;9:1441.
41. Hazhir N, Chekin F, Raoof JB, Fathi SH. A porous reduced graphene oxide/chitosan-based nanocarrier as a delivery system of doxorubicin. RSC Adv. 2019;9:30729–35.
42. Batista Deroco P, Campanhã Vicentini F, Gabriel Oliveira G, Rocha-Filho RC, Fatibello-Filho O. Square wave voltammetric determination of hydroxychloroquine in pharmaceutical and synthetic urine samples using a cathodically pretreated boron-doped diamond electrode. J Electroanal Chem. 2014;719:19–23.
43. Ghoreishi SM, Attaran AM, Amin AM, Khoobi A. Multiwall carbon nanotube modifed electrode as a nanosensor for electrochemical studies and stripping voltammetric determination of an antimalarial drug. RSC Adv. 2015;5:14407–15.
44. Carvalho MS, Rocha RG, de Faria LV, Richter EM, Dantas LMF, da Silva IS, et al. Additively manufactured electrodes for the electrochemical detection of hydroxychloroquine. Talanta. 2022;250:123727.
45. Khoobi A, Ghoreishi SM, Behpour M. Sensitive and selective determination of hydroxychloroquine in the presence of uric acid using a new nanostructure self-assembled monolayer modified electrode: Optimization by multi variated at an analysis. Analyst. 2014;139:4064–72.
46. Khoobi A, Ghoreishi SM, Behpour M, Shaterian M, Salavati-Niasari M. Design and evaluation of a highly sensitive nanostructure-based surface modification of glassy carbon electrode for electrochemical studies of hydroxychloroquine in the presence of acetaminophen. Colloids Surf B. 2014; 123:648–56.
47. Celik TA, Aslanturk OS, Yilmaz ES, Guzel Y. Antioxidant and cytotoxic activities of Fumaria parviflora lam. and Fumaria capreolata L. KSÜ Tarım ve Doğa Derg 2022;25:819–27.
48. Si X, Wei Y, Wang C, Li L, Ding Y. A sensitive electrochemical sensor for ofloxacin based on a graphene/zinc oxide composite film. Anal Methods. 2018;10:1961–7.
49. Wang Q, Yue H, Zhang J, Gao X, Zhang H, Lin X, et al. Electrochemical determination of uric acid in the presence of ascorbic acid by hybrid of ZnO nanorods and graphene nanosheets. Ionics. 2017;24:2499–507.
50. Liu Y, Xiao Y, Zhang Y, Gao X, Wang H, Niu B, Li W. ZnO-rGO-based electrochemical biosensor for the detection of organophosphorus pesticides. Bioelectrochem. 2024;156:108599.
51. Bum Kang S, Sanger A, Jeong MH, Baik JM, Jin Choi K. Heterogeneous stacking of reduced graphene oxide on ZnO nanowires for NO_2 gas sensors with dramatically improved response and high sensitivity. Sens Actuators B. 2023;379:133196.